

Active versus passive squeezing by second-harmonic generation

Andrew G. White, Tim C. Ralph, and Hans-A. Bachor

Department of Physics, The Faculties, The Australian National University, Canberra 0200, Australia

Received May 19, 1995; revised manuscript received December 22, 1995

The characteristics of squeezed light generated by both passive (occurring in a cavity external to a laser) and active (occurring within a laser cavity) second-harmonic generation (SHG) are investigated and contrasted. Squeezing of both the fundamental and the second harmonic is discussed, and the issue of doubly versus singly resonant behavior is addressed. We examine passive squeezing by explicitly modeling the intrinsically noisy output of the pump laser and coupling it to a passive, multiport, lossy SHG cavity. Low-frequency degradation of the squeezing caused by the laser pump noise is predicted and provides a probable explanation for previous discrepancies between theory and experiment. Active squeezing is quantitatively modeled by a three-level laser model that retains all laser dynamics. Previously disparate predictions are reconciled. For one parameter set two regimes of squeezing are predicted: 50% squeezing at frequencies lower than the laser relaxation oscillation, and near-perfect squeezing at frequencies above. A particular problem of active squeezing is highlighted: The fast dephasing of the laser coherence introduces considerable excess noise likely to mask squeezing in experimental situations. We conclude that, although passive SHG is a practical source of squeezing, active SHG is unlikely to be so in the foreseeable future. © 1996 Optical Society of America

1. INTRODUCTION

As one of the simplest nonlinear optical processes, second-harmonic generation (SHG) has been extensively investigated and successfully used as a source of nonclassical light. In this paper we present models for both active (occurring within a laser cavity) and passive (occurring in a cavity external to a laser) SHG that include the effect of noise from the laser. In particular, we evaluate the squeezing available with Nd:YAG as an active gain medium and investigate which experimental approaches are the most promising.

Perfect amplitude squeezing of either the fundamental or the second harmonic, depending on the relative loss rates,¹⁻² has been predicted for a passive, doubly resonant, lossless SHG cavity. In the experimentally simpler case of a cavity resonant solely at the fundamental it is still theoretically possible to obtain maximum squeezing at the second harmonic of 1/9.³ Given the allure of a bright, intensely squeezed source, there has been an increasing amount of experimental work in this field. Recent results include direct observations of as much as 52% noise reduction in the fundamental^{4,5} and 30% noise reduction in the second harmonic.^{3,6} The strong correlation between the fundamental and the second harmonic has also been proposed as the basis of a quantum non-demolition measurement scheme.⁷

Most treatments of squeezing in passive SHG to date have concentrated on the ideal regime, i.e., single-ended, lossless systems that can attain extreme nonlinearities, with a coherent pump or with idealized laser phase noise.⁸ There have been marked discrepancies between theory and experiment.³ Our model allows a quantitative comparison between theory and experiment by extending previous treatments in two ways. First, we explicitly consider the optimum squeezing available for a multi-

port, lossy system with achievable or near-achievable nonlinearities. Second, we explicitly model the pump as the intrinsically noisy output of a laser. For the case of singly resonant passive SHG, we compared our model with experimental results⁶ and found excellent agreement. In this paper we use our model to investigate and compare the other experimental cases.

Active SHG, in which the doubling crystal is placed inside the laser cavity, has been examined theoretically. In the *good-cavity* limit, in which the atomic decay rates are much higher than the relevant field decay rates, as is the case for a gas laser, the system is modeled by adiabatic elimination of the atomic variables.⁹ This introduces broadband atomic noise, which degrades the correlation between the amplitudes of the second harmonic and the fundamental. Nevertheless, a maximum of 50% squeezing of the amplitude of the second harmonic has been predicted, with an optimum value at zero frequency and decreasing with frequency. This has been elegantly explained as the Poissonian photons of the fundamental being converted with high efficiency to second-harmonic photons, which consequently have half-Poissonian statistics.¹⁰ In the *bad-cavity* limit, in which the field decay rate of the mode of interest is much greater than the atomic decay rate and the decay rate of the other mode,^{11,12} the bandwidth of the atomic noise is small and there is a high correlation between the amplitude of the second harmonic and the fundamental. Appropriate interaction between the two cavity modes allows perfect squeezing at nonzero frequencies. To the best of the authors' knowledge, no treatment to date has reconciled these two regimes within the one model.

Previously, active SHG has been studied with either the Haken-Lamb or the Lax-Louisell laser models. The Haken-Lamb model retains all the laser dynamics of a two-level system. However, for many lasers it is not pos-

sible to describe the threshold behavior correctly with a two-level model. The Lax–Louisell model is a three-level system in which the lasing coherence is adiabatically eliminated. Unfortunately, some interesting dynamical behavior is lost in this limit. In this paper we use a three-level model¹³ similar to the Lax–Louisell model except that it retains all laser dynamics explicitly.

Perfect squeezing can be achieved only when there is a strong interaction between the fundamental and the second harmonic. Experimentally this dictates a doubly resonant system. Passive doubly resonant SHG systems are technically complicated, as passive cavities require locking systems to remain resonant. To highlight this, consider that Kürz *et al.*,⁴ who obtained 52% squeezing, could maintain double resonance for only as long as 10 s. This compares poorly to passive singly resonant systems, which can be maintained on lock for hours. As active modes are automatically resonant, there is a strong experimental attraction to active SHG, as it requires locking of, at most, only the second-harmonic cavity. It promises strong squeezing in technically elegant systems.

This paper is arranged as follows. In Section 2 we develop our models of active and passive SHG. Section 3 discusses modeling specific experiments and lists the numerical values used in the remainder of the paper. In Section 4 we explore and tabulate the regimes of squeezing, with particular reference to the effect of nonzero laser dephasing. Finally, the experimental implications and a discussion of the results are given in Section 5.

2. THEORY

A. Hamiltonians and Master Equations

Figures 1(a) and 1(b) are schematics of passive and active second-harmonic generation, respectively. The same laser model is used for both, and consists of N three-level atoms interacting with an optical ring-cavity mode through the resonant Jaynes–Cummings Hamiltonian. In the interaction picture this is

$$\hat{H}_{\text{laser}} = i\hbar g_{23} \sum_{\mu=1}^N (\hat{a}^\dagger \hat{J}_{23}^- - \hat{a} \hat{J}_{23}^+), \quad (1)$$

where carets indicate operators, g_{23} is the dipole coupling strength between the atoms and the cavity, \hat{a} and \hat{a}^\dagger are the lasing-mode annihilation and creation operators, and \hat{J}_{23}^+ and \hat{J}_{23}^- are the collective Hermitian-conjugate lowering and raising operators between the $|i\rangle$ th and the $|j\rangle$ th levels of the lasing atoms. Level 1 is the ground level. The field phase factors are absorbed into the definition of the atomic operators.

For the passive case the standard Hamiltonian for SHG is used¹:

$$\hat{H}_{\text{shgl}} = i\hbar \frac{\chi}{2} (\hat{b}^\dagger \hat{c} - \hat{b} \hat{c}^\dagger), \quad (2a)$$

where \hat{b} and \hat{b}^\dagger are the fundamental annihilation and creation operators, \hat{c} and \hat{c}^\dagger are the second-harmonic annihilation and creation operators, and χ is the coupling parameter for the interaction between the two modes. For the active case the Hamiltonian is essentially the same,

except now the fundamental and the lasing modes are one and the same, so that

$$\hat{H}_{\text{shg2}} = i\hbar \frac{\chi}{2} (\hat{a}^\dagger \hat{c} - \hat{a} \hat{c}^\dagger), \quad (2b)$$

where the other terms are as above.

For both cases, standard techniques¹⁴ are used to couple the lasing atoms and the cavities to reservoirs and to derive a master equation for the reduced density operator $\hat{\rho}$ of the system. Included in the laser model are spontaneous atomic emission from level $|3\rangle$ to level $|2\rangle$, and from level $|2\rangle$ to level $|1\rangle$, at rates γ_{23} and γ_{12} , respectively. Incoherent pumping of the laser occurs at a rate Γ ; the rate of collisional- or lattice-induced phase decay of the lasing coherence is γ_p .

In general, optimum squeezing in these systems occurs at zero detuning. Because of space constraints, we do not examine the effect of non-zero detunings in this paper: all detunings are set to zero. However, in passing we mention the varied effects of detuning: the quadrature of the squeezing can be rotated^{15–17}; the squeezing can be degraded as the intracavity intensity is lowered, and less power is available to drive the nonlinearity; the form of the nonlinearity can change¹; and the stability point of the system can move.⁹ To date, experimenters have found it possible to lock with sufficient accuracy such that nonzero detunings need not be considered,^{3,6} or they have obtained results by scanning the detuning,^{4,5} allowing observation of the zero detuning point. In both situations it has been found that the theories with zero detuning model the results satisfactorily.

In the passive case the driving of the SHG cavity by the laser is modeled with the cascaded quantum system formalism of Carmichael¹⁸ and Gardiner.¹⁹ The laser-cavity damping rate of the output port that pumps the passive cavity is $2\kappa_a$; the cavity decay rate for the fundamental mode of the passive cavity is $2\kappa_b$; and the cavity decay rate for the second-harmonic mode is $2\kappa_c$. The resulting interaction-picture master equation is

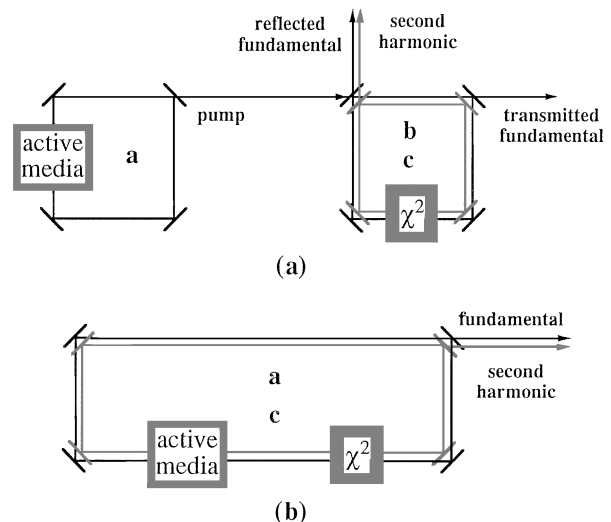


Fig. 1. Schemata of (a) passive and (b) active second-harmonic generation: a, the lasing mode; b, the fundamental mode of the SHG cavity; and c, the second-harmonic mode.

$$\begin{aligned}
\frac{\partial}{\partial t} \hat{\rho} &= \frac{1}{i\hbar} [\hat{H}_{\text{laser}}, \hat{\rho}] + \frac{1}{i\hbar} [\hat{H}_{\text{shg1}}, \hat{\rho}] \\
&+ \frac{1}{2} (\gamma_{12} L_{12} + \gamma_{23} L_{23}) \hat{\rho} + \frac{\Gamma}{2} (L_{13} \rho)^\dagger \\
&+ \frac{1}{4} \gamma_p [2(\hat{J}_3 - \hat{J}_2) \hat{\rho} (\hat{J}_3 - \hat{J}_2) \\
&- (\hat{J}_3 - \hat{J}_2)^2 \hat{\rho} - \hat{\rho} (\hat{J}_3 - \hat{J}_2)^2] \\
&+ \kappa_a (2\hat{a} \hat{\rho} \hat{a}^\dagger - \hat{a}^\dagger \hat{a} \hat{\rho} - \hat{\rho} \hat{a}^\dagger \hat{a}) \\
&+ \kappa_b (2\hat{b} \hat{\rho} \hat{b}^\dagger - \hat{b}^\dagger \hat{b} \hat{\rho} - \hat{\rho} \hat{b}^\dagger \hat{b}) \\
&+ \kappa_c (2\hat{c} \hat{\rho} \hat{c}^\dagger - \hat{c}^\dagger \hat{c} \hat{\rho} - \hat{\rho} \hat{c}^\dagger \hat{c}) \\
&+ 2\sqrt{\kappa_a \kappa_b} (\hat{a} \hat{\rho} \hat{b}^\dagger + \hat{b} \hat{\rho} \hat{a}^\dagger - \hat{\rho} \hat{a}^\dagger \hat{b} - \hat{\rho} \hat{a} \hat{b}^\dagger), \\
L_{ij} \hat{\rho} &= (2\hat{J}_{ij}^- \hat{\rho} \hat{J}_{ij}^+ - \hat{J}_{ij}^+ \hat{J}_{ij}^- \hat{\rho} - \hat{\rho} \hat{J}_{ij}^+ \hat{J}_{ij}^-). \quad (3a)
\end{aligned}$$

Similarly, in the active case the fundamental cavity damping rate is $2\kappa_a$, and the cavity decay rate for the second-harmonic mode is $2\kappa_c$. The interaction-picture master equation is

$$\begin{aligned}
\frac{\partial}{\partial t} \hat{\rho} &= \frac{1}{i\hbar} [\hat{H}_{\text{laser}}, \hat{\rho}] + \frac{1}{i\hbar} [\hat{H}_{\text{shg2}}, \hat{\rho}] \\
&+ \frac{1}{2} (\gamma_{12} L_{12} + \gamma_{23} L_{23}) \hat{\rho} + \frac{\Gamma}{2} (L_{13} \rho)^\dagger \\
&+ \frac{1}{4} \gamma_p [2(\hat{J}_3 - \hat{J}_2) \hat{\rho} (\hat{J}_3 - \hat{J}_2) \\
&- (\hat{J}_3 - \hat{J}_2)^2 \hat{\rho} - \hat{\rho} (\hat{J}_3 - \hat{J}_2)^2] \\
&+ \kappa_a (2\hat{a} \hat{\rho} \hat{a}^\dagger - \hat{a}^\dagger \hat{a} \hat{\rho} - \hat{\rho} \hat{a}^\dagger \hat{a}) \\
&+ \kappa_c (2\hat{c} \hat{\rho} \hat{c}^\dagger - \hat{c}^\dagger \hat{c} \hat{\rho} - \hat{\rho} \hat{c}^\dagger \hat{c}). \quad (3b)
\end{aligned}$$

B. Semiclassical Equations

The semiclassical equations of motion are obtained directly from the master equation by the approximation of factorizing expectation values.

1. Passive Case

The semiclassical equations of motion for the passive case are

$$\dot{J}_{23} = g_{23}(J_3 - J_2)a - \frac{1}{2}(\gamma_{23} + \gamma_{12} + 2\gamma_p)J_{23}, \quad (4)$$

$$\dot{J}_2 = g_{23}(J_{23}a^\dagger - \hat{J}_{23}^+ a) + \gamma_{23}J_3 - \gamma_{12}J_2, \quad (5)$$

$$\dot{J}_3 = -g_{23}(J_{23}a^\dagger - \hat{J}_{23}^+ a) + \Gamma J_1 - \gamma_{23}J_3, \quad (6)$$

$$\dot{a} = g_{23}J_{23} - \kappa_a a, \quad (7)$$

$$\dot{b} = \chi b^\dagger c - (\kappa_b + i\Delta_b)b - 2\sqrt{\kappa_a \kappa_b} a, \quad (8)$$

$$\dot{c} = -\kappa_c c - \frac{\chi}{2} b^2, \quad (9)$$

and their conjugate equations. The absence of circumflexes indicate semiclassical expectation values. Here κ_a is the total loss rate of the laser cavity; κ_b is the total loss rate of the fundamental light; κ_c is the total loss rate of the second-harmonic light; and χ is the coupling constant between fundamental and the second harmonic. We use the following standard scaling with the number of atoms N :

$$\begin{aligned}
\tilde{a} &= \frac{a}{\sqrt{N}}, & \tilde{b} &= \frac{b}{\sqrt{N}}, & \tilde{\chi} &= \chi\sqrt{N}, & \tilde{g}_{23} &= g_{23}\sqrt{N}, \\
\tilde{J}_i &= \frac{J_i}{N}, & \tilde{J}_{ij} &= \frac{J_{ij}}{N}. \quad (10)
\end{aligned}$$

2. Active Case

In the active case, Eqs. (4)–(6) are unchanged; however, the equations for the fundamental and the second-harmonic modes become

$$\dot{a} = g_{23}J_{23} - \kappa_a a + \chi a^\dagger c, \quad (11a)$$

$$\dot{c} = -\kappa_c c - \frac{\chi}{2} a^2, \quad (11b)$$

and their conjugate equations. We obtain the conditions for semiclassical steady state by setting derivatives to zero.

C. Noise Spectra

The drift and the diffusion matrices are listed in Appendix A. Their calculation, by obtention of c -number Fokker–Planck equations from the master equation with positive- p representation, is standard.²⁰ We assume that the quantum fluctuations are sufficiently small that the full solutions can be written in the form

$$\tilde{a}(t) = a_0 + \delta a, \quad \tilde{b}(t) = b_0 + \delta b, \quad \tilde{c}(t) = c_0 + \delta c, \quad (12)$$

where a_0 is the semiclassical steady state. For brevity we use a, b, \dots , to mean the scaled steady-state solutions, e.g., $a \equiv \tilde{a}_0$. The spectral matrix $S(\omega)$ is defined as the Fourier-transformed matrix of the two time correlation functions of these small quantum perturbations ($\delta \tilde{\alpha}_j$) about the semiclassical steady state, i.e.,

$$S_{ij} = \int_{-\infty}^{\infty} \exp(i\omega t) \langle \delta \alpha_i(t + \tau), \delta \alpha_j(t) \rangle d\tau_i. \quad (13)$$

The ordering of the perturbations for the passive and the active cases, respectively, is

$$\delta \alpha = (\delta a, \delta a^\dagger, \delta b, \delta b^\dagger, \delta c, \delta c^\dagger, \delta J_{23}^-, \delta J_3, \delta J_2, \delta J_{23}^+), \quad (14a)$$

$$\delta \alpha = (\delta a, \delta a^\dagger, \delta c, \delta c^\dagger, \delta J_{23}^-, \delta J_2, \delta J_{23}^+). \quad (14b)$$

The spectral matrix may be calculated from the Fokker–Planck equations in both cases. The solution for the spectral matrix is

$$S(\omega) = (A - i\omega I)^{-1} D (A^\dagger + i\omega I)^{-1}. \quad (15)$$

The drift, A , and the diffusion, D , matrices are listed in Appendix A. The squeezing spectrum is then defined by

$$V(X_\theta, \omega) = \int_{-\infty}^{\infty} \exp(i\omega t) \langle X_\theta(t + \tau), X_\theta(t) \rangle d\tau, \quad (16)$$

where we use the notation $\langle X, Y \rangle = \langle XY \rangle - \langle X \rangle \langle Y \rangle$. We obtain noise spectra for modes, a, b , or c by defining the quadrature phase amplitude of the transmitted field z as

$$X_\theta(t) = z_{\text{out}}(t) \exp(-i\theta) + z_{\text{out}}^\dagger(t) \exp(i\theta), \quad (17)$$

where z represents modes a, b , or c . Setting $\theta = 0$ gives the amplitude noise spectra; provided the quantum perturbations are small, these spectra are equivalent to those observed by direct detection of the beams.

Using the input/output formalism of Collett and Gardiner,²¹ we are able to obtain the spectra in terms of the spectral matrix $S(\omega)$. In the passive case, using the ordering of Eq. 14(a), we obtain for the laser, the transmitted fundamental, and the second harmonic, respectively,

$$\begin{aligned} V_{\text{laser}} &= 1 + 2\kappa_a[S_{12}(\omega) + S_{21}(\omega) \\ &\quad + \exp(-2i\theta)S_{11}(\omega) \\ &\quad + \exp(2i\theta)S_{22}(\omega)], \\ V_{\text{transmitted fundamental}} &= 1 + 2\kappa_{b2}[S_{78}(\omega) + S_{87}(\omega) \\ &\quad + \exp(-2i\theta)S_{77}(\omega) \\ &\quad + \exp(2i\theta)S_{88}(\omega)], \\ V_{\text{second harmonic}} &= 1 + 2\kappa_c[S_{910}(\omega) + S_{109}(\omega) \\ &\quad + \exp(-2i\theta)S_{99}(\omega) \\ &\quad + \exp(2i\theta)S_{1010}(\omega)], \end{aligned} \quad (18)$$

where κ_{b2} is the loss rate of a fundamental mirror that is *not* the pump mirror.

The spectrum of the reflected fundamental depends on both the noise of the laser mode and the noise of the fundamental. The amplitude spectrum is thus given by

$$\begin{aligned} V_{\text{reflected fundamental}} &= 1 + 2\kappa_{b1}[S_{78}(\omega) + S_{87}(\omega) + S_{77}(\omega) + S_{88}(\omega)] \\ &\quad + 2\kappa_a[S_{12}(\omega) + S_{21}(\omega) + S_{11}(\omega) + S_{22}(\omega)] \\ &\quad + 2\sqrt{\kappa_{b1}\kappa_a} \left[\begin{array}{l} S_{71}(\omega) + S_{72}(\omega) + S_{82}(\omega) + S_{81}(\omega) \\ + S_{17}(\omega) + S_{18}(\omega) + S_{27}(\omega) + S_{28}(\omega) \end{array} \right]. \end{aligned} \quad (19)$$

In the active case, using the ordering of Eq. 14(b), we obtain spectra for the fundamental and the second harmonic, respectively, as

$$\begin{aligned} V_{\text{fundamental}} &= 1 + 2\kappa_a[S_{12}(\omega) + S_{21}(\omega) \\ &\quad + \exp(-2i\theta)S_{11}(\omega) + \exp(2i\theta)S_{22}(\omega)], \\ V_{\text{second harmonic}} &= 1 + 2\kappa_c[S_{78}(\omega) + S_{87}(\omega) \\ &\quad + \exp(-2i\theta)S_{77}(\omega) + \exp(2i\theta)S_{88}(\omega)]. \end{aligned} \quad (20)$$

with Eq. (15), spectra can thus be generated numerically.

3. MODELING OF EXPERIMENTS AND NUMERICAL PARAMETERS

We are particularly interested in experimental systems pumped by Nd:YAG lasers. Although Nd:YAG lasers are four-level systems, we can model them accurately with a three-level model, as the decay rate from the fourth to the third level is very much faster (approximately ten-fold) than the other decay rates of the system, and so it has negligible effects on the dynamics of the system. Accordingly, we use the following values:

$$\begin{aligned} \gamma_{23} &= 5 \times 10^{-5} \gamma_{12}, & \gamma_{13} &= 2\gamma_{23} \gamma_{12}, \\ \gamma_{\text{tot}} &= (\gamma_p + \gamma_{13} + \gamma_{23} + 1)\gamma_{12}, \\ \sigma &= 6.5 \times 10^{-23} \text{ m}^2, & \gamma_p &= 9000\gamma_{12}, \\ g_{23} &= [(c'\sigma\rho\gamma_{\text{tot}})/4]^{1/2}, \end{aligned} \quad (21)$$

where the speed of light in Nd:YAG is $c' = 1.64 \times 10^8 \text{ ms}^{-1}$, the density of Nd atoms in Nd:YAG is $\rho = 1.38 \times 10^{26} \text{ atoms m}^{-3}$, and σ is the stimulated emission cross section. The decay rate from level 2 to 1 is $\gamma_{12} = 1/(30 \times 10^{-9}) \text{ s}^{-1}$.

Please note that, although the expressions for squeezing spectra are given in terms of angular frequency ($[\omega] = \text{rads}^{-1}$), the decay rates are in expressed in hertz ($[f] = \text{s}^{-1}$), as is customary. All spectra in this paper are plotted in hertz (s^{-1}).

We also wish to model the lossy, multiport nature of experimental cavities. Let the total loss rate for a cavity be given by

$$\kappa_\mu = \kappa_{\mu 1} + \kappa_{\mu 2} + \kappa_{\text{abs in } \mu}, \quad (22)$$

where μ is the mode, either a , b , or c ; the first two terms are the loss rates through the first and the second mirrors, respectively; and the last term is the loss rate that is due to absorption. The mirror loss rates are related to the mirror transmissions $T_{\mu i}$ by

$$\kappa_{\mu i} = \frac{c'T_{\mu i}}{2p}, \quad (23)$$

where i represents the first or the second mirror, respectively; p is the geometrical cavity perimeter. The loss rate that is due to absorption is given by

$$\kappa_{\text{abs in } \mu} = -\frac{c'}{2p} \log[\exp(-\alpha_0 l)], \quad (24)$$

where α_0 is the absorption loss per unit distance and l is the physical crystal length.

The interaction is scaled by the number of lasing atoms, as shown in Eq. (10). The number of lasing atoms, N , can be estimated one of two ways. The first is to calculate the effective mode volume and then to use the known density of Nd atoms in YAG ($\rho = 1.38 \times 10^{20} \text{ atoms cm}^{-3}$). An alternative is to use an expression for the output power:

$$P_{\text{laser}} = 2h\nu N \gamma_{12} \kappa_a^{\text{out}} a^2, \quad (25)$$

where h is Planck's constant; ν is the laser frequency; and κ_a^{out} is the loss rate of the laser output mirror. Using the measured laser power, we determine the number of atoms by Eq. (25) as $N = 10^{17}$.

The models presented here are for doubly resonant systems. This approach allows exploration of various squeezing regimes by smoothly varying the interaction between the modes. In order to model singly resonant systems, we simply take the appropriate bad-cavity limit. In this way the results of an explicitly singly resonant theory (such as Paschotta *et al.*³) can be exactly duplicated without loss of generality.

4. REGIMES OF SQUEEZING

Table 1 summarizes the results. The optimum predicted squeezing for both active and passive SHG is considered for the two principal configurations: singly resonant at the fundamental frequency, ω , and doubly resonant. Two limits of the squeezing are considered: *ideal* and *realistic with pump noise*. The ideal

Table 1. Summary of Degree and Frequency of Optimum Squeezing in the Various Regimes of Second-Harmonic Generation with Reference to the Figures; Frequencies Are Scaled by γ_{12} , the Decay Rate from Level 2 to 1 in the Active Medium

Mode	Passive				Active			
	Ideal Limit ^a		Realistic with Pump Noise ^b		Ideal Limit ^a		Realistic with Pump Noise ^b	
	2ω	ω	2ω	ω	2ω	ω	2ω	ω
Singly resonant case (at ω) ^c	Fig. 2(a) $V_{\text{opt}} = 1/9$ $V_{\text{opt}} = 2/3$		Fig. 2(b) $V_{\text{opt}} \cong 0.5$ $V_{\text{opt}} \cong 0.95$		Fig. 5 $V_{\text{opt}} = 1/2$ $V_{\text{opt}} = 1/2$		No squeezing owing to high γ_p	No squeezing owing to high γ_p
	$\Omega_{\text{opt}} = 0$	$\Omega_{\text{opt}} = 0$	$\Omega_{\text{opt}} \cong 1.1\gamma_{12}$	$\Omega_{\text{opt}} \cong 1.2\gamma_{12}$	$\Omega_{\text{opt}} = 0$	$\Omega_{\text{opt}} = 0$		
Doubly resonant case	Fig. 3(a) $V_{\text{opt}} = 0$	Fig. 4(a) $V_{\text{opt}} = 0$	Fig. 3(b) $V_{\text{opt}} \cong 0.1$	Fig. 4(b) $V_{\text{opt}} \cong 0.3$	Fig. 6 $V_{\text{opt}} = 0$	Not illustrated $V_{\text{opt}} = 0$	Fig. 9 $V_{\text{opt}} \cong 1/2$	No squeezing owing to high γ_p
	$\Omega_{\text{opt}} \neq 0$	$\Omega_{\text{opt}} \neq 0$	$\Omega \cong 1.5\gamma_{12}$	$\Omega \cong 0.5\gamma_{12}$	$\Omega_{\text{opt}} \neq 0$	$\Omega_{\text{opt}} \neq 0$	$\Omega_{\text{opt}} \neq 0$	

^aThe ideal limit to squeezing comes from consideration of a coherently pumped single-ended lossless device and is included for ease of comparison with previous literature. However, all plots in the ideal-limit column come from consideration of the experimentally applicable case of a coherently pumped, multiport, lossy device.

^bThe realistic-with-pump-noise limit comes from consideration of the experimental case of a multiport, lossy device pumped by an intrinsically noisy Nd:YAG laser. It is not a limit in the sense that these figures cannot be bettered—it simply summarizes the effect of laser noise, as shown in the referenced plots.

^cMore accurately, this is the bad-cavity limit of 2ω . The 2ω singly resonant case is not considered in this table, because effectively, the corresponding bad-cavity limit (for ω) cannot be reached. To see squeezing in the later case requires high pump powers that drive the interaction toward the doubly resonant limit, as in Fig. 8.

limit comes from consideration of a coherently pumped, single-ended, lossless device, and it is included for easy comparison with previous theoretical literature. However, the plots referenced in the ideal column come from consideration of the experimentally applicable case of a coherently pumped multiport, lossy device. Thus, for example, Fig. 2(a) has a limiting value 0.28 and not 1/9 as given in the table. The difference is due to the fraction of the squeezing that goes unobserved because it is either absorbed within the cavity or exits through the other port.

The realistic with pump noise limit comes from consideration of the experimental case of a multiport, lossy device pumped by a Nd:YAG laser. It is not a limit in the sense that these figures cannot be bettered—it simply summarizes the effect of laser noise as shown in the plots and provides a realistic guide to the noise suppression that can be expected. In addition, the typical detection frequencies at which the best noise suppression occurs are listed in Table 1. They indicate the optimum point of operation for a squeezing experiment and are given as multiples of the linewidth of the SHG cavity at the fundamental ω .

A. Passive Second-Harmonic Generation

1. Squeezing of Second-Harmonic Light

Good squeezing of the second harmonic requires that the second-harmonic loss rate be higher than that of the fundamental cavity, i.e., $\kappa_c > \kappa_b$. However, to obtain perfect squeezing, it is not desirable that κ_c be arbitrarily larger than κ_b . To see this, we first consider the singly resonant case (or the bad-cavity limit for 2ω), $\kappa_c \gg \kappa_b$. Figure 2(a) shows the noise spectrum with a coherent pump: The maximum squeezing occurs at zero frequency, in the vicinity of the optimum value of 1/9, and then degrades with frequency. Perfect squeezing cannot be achieved. If a laser pump is used, as shown

in Fig. 2(b), the situation degrades further owing to the large amounts of low-frequency noise added by the laser. This effectively moves the maximum squeezing out in frequency while reducing its value. These results suggest a partial explanation for the results of Paschotta *et al.*³ They observed a deviation between theory and experiment that increased as a function of power. This can be simply explained by our model as the noise tail of the laser masking the squeezing. As the power is increased, so does the laser noise. The other behaviors noted by Paschotta *et al.* and attributed to thermal effects (an apparent bistability with degraded squeezing on one

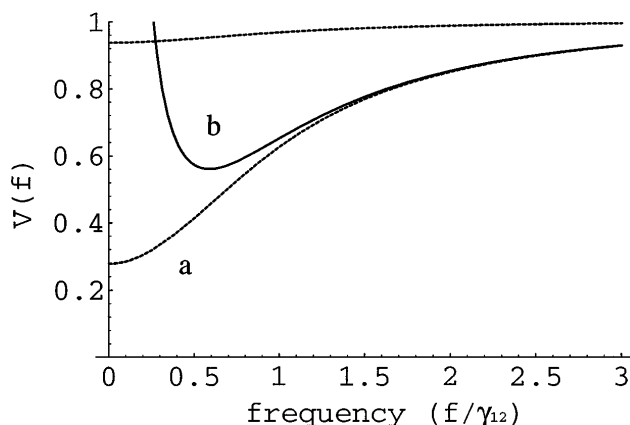


Fig. 2. Spectra for passive SHG in the singly resonant case. The parameters are optimized to squeeze the second harmonic, i.e., $\kappa_c \gg \kappa_b$, where $\kappa_b = 0.604\gamma_{12}$ and $\kappa_c = 77.6\gamma_{12}$, and scaled nonlinearity $\chi = 120\,000$ (approximately $12\,600\text{ s}^{-1}$ unscaled), for a pump power of 120 mW. The frequency axis is scaled by $\gamma_{12} = 33.3\text{ MHz}$. a, Dashed curve, spectra obtained with a coherent pump. The lower trace is the second harmonic, and the upper trace is the fundamental. b, Solid curve, second-harmonic spectrum obtained with a laser pump. The squeezing is masked at low frequencies.

branch, a consistent point of degraded squeezing) may be caused by parasitic parametric operation.²²

How then can perfect squeezing be obtained? Consider the doubly resonant case. It is well known that as a doubly resonant system is driven toward the critical point that marks the onset of self-pulsing, a damped oscillation occurs in the phase quadrature of the second harmonic. At the critical point this turns into the self-pulsing frequency. Below the critical point, the squeezing is enhanced at the frequency of the damped oscillation with a maximum noise suppression close to the critical point. Thus to obtain perfect squeezing, we need to force the system close to the critical point. We can do this by increasing the power or nonlinearity or by adjusting the cavity decay rates so that the two modes interact more strongly.

Consideration of the phase oscillation gives, after solving the linearized semiclassical equations, the frequency for the maximum amplitude squeezing

$$\omega_{sq} \approx \left\{ \frac{\kappa_c(2\kappa_b)a}{b} - 2\kappa_b\kappa_c - \left[\frac{\kappa_b}{2} + \kappa_1 + \frac{(2\kappa_1)^{1/2}a}{2b} - \frac{c^2b^2}{\kappa_c} \right]^2 \right\}^{1/2}. \quad (26)$$

Figures 3(a) and 3(b) clearly show this effect for coherent and laser pumps, respectively.

2. Squeezing of the Fundamental Light

While much of the behavior discussed for the second harmonic applies to the fundamental, the two modes are by no means identical. Experimentally, it would be possible to build a frequency-doubler resonant only at the second harmonic, but in cw operation, unrealistically high fundamental pump powers are then necessary to drive the doubling process. A high-finesse cavity for the fundamental light is employed to build up sufficient power. However, as good squeezing of the fundamental requires that the fundamental cavity be lossier than that of the second harmonic ($\kappa_b > \kappa_c$), a doubly resonant system is necessary. This is confirmed by the rather poor noise suppression of the fundamental light shown in Figs. 2 and 3.

Spectra of the fundamental light from a doubly resonant passive doubler, for both coherent and laser pumps, are shown in Figs. 4(a) and 4(b), respectively. For the coherent pump the squeezing at zero frequency is modest (the maximum possible value is 2/3); however, owing to the strong interaction between the modes [despite the relative difference in loss rates; c.f. Fig. 2(a)], there is a large oscillation that dips to nearly zero. Note that the fundamental spectra in this figure are for a cavity in which the fundamental is strongly transmitted (c.f. Fig. 1). The distinction is important when there is a noisy pump beam. In general the reflected beam consists of two components, the part that interacts with the cavity (the *impedance-matched* component) and the part that is reflected off the cavity without interacting. This latter component contributes additional noise to the reflected beam that can mask the squeezing.

For a given power in the second-harmonic case the squeezing is optimized as the interaction is strengthened (i.e., χ is increased). Strikingly, this is not the case for the fundamental. At a given pump power the squeezing degrades for $\chi \rightarrow \infty$. There is an optimum value for

the coupling parameter χ . For sufficiently large χ the squeezing is degraded at all detection frequencies. This can be understood with the following analogy. Consider the frequency doubler as a nonlinear beam splitter, with an incident fundamental beam split into, say, a transmitted fundamental beam and a reflected second-harmonic beam. The squeezing on the incident fundamental is directly proportional to χ . As χ is increased, the squeezing on the incident fundamental increases, and, importantly, the reflectivity of the beam splitter increases. Thus in the limit of infinite χ , all of the incident fundamental becomes second harmonic, which is strongly squeezed. Conversely, as χ is increased, the fraction of the incident

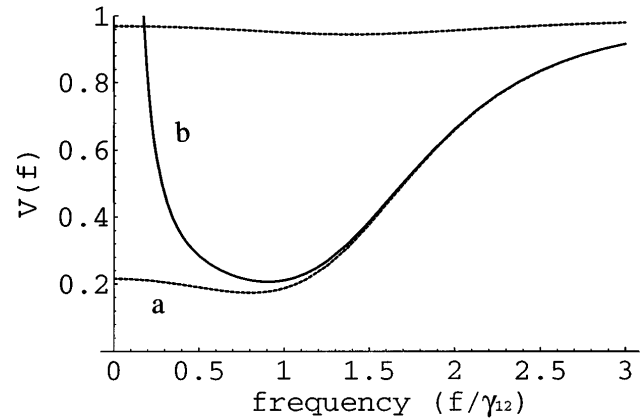


Fig. 3. Spectra for passive SHG in the doubly resonant case. The parameters are optimized to squeeze the second harmonic and are as for Fig. 2, except here $\kappa_c = 9.06\gamma_{12}$. a, Dashed curve, spectra obtained with a coherent pump. The lower trace is the second harmonic, and the upper trace is the fundamental. The squeezing on the second harmonic is much improved with no increase in interaction strength or pump power. b, Solid curve, second-harmonic spectrum obtained with a laser pump. Again, the squeezing is masked at low frequencies.

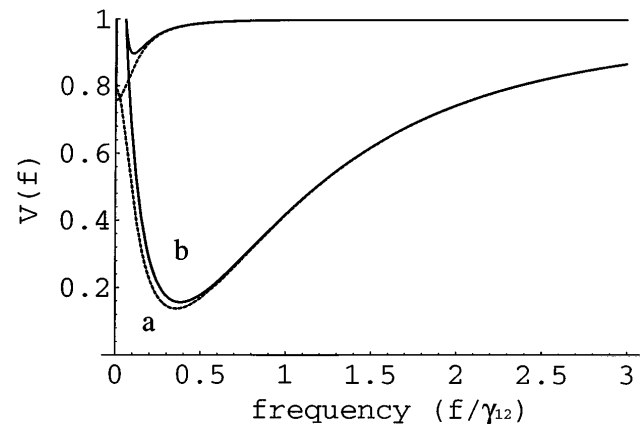


Fig. 4. Spectra for passive SHG in the doubly resonant case. The parameters are optimized to squeeze the fundamental, i.e., $\kappa_b > \kappa_c$, where $\kappa_b = 3.46\gamma_{12}$ and $\kappa_c = 0.362\gamma_{12}$. The interaction and the pump power are the same as for Figs. 2 and 3. a, Dashed curve, spectra obtained with a coherent pump. The lower trace is the fundamental, and the upper trace is the second harmonic. The fundamental is squeezed well beyond the 2/3 limit of the singly resonant case. In the appropriate ideal case, perfect squeezing is possible. b, Solid curves, spectra obtained with a laser pump. The squeezing is destroyed at low frequencies. The lower trace is the fundamental, and the second harmonic trace is above shot noise and is thus not visible on this plot.

fundamental that is transmitted (i.e., light remaining at the fundamental wavelength) becomes less and less, with a concomitant decrease in the squeezing.

B. Active Second-Harmonic Generation

1. Squeezing of the Second-Harmonic Light

For clarity we first consider active SHG under the assumption that the atomic dephasing rate, γ_p , is zero (Subsection 4.C explains why this is desirable). Consider squeezing of the second harmonic in the singly resonant limit, $\kappa_c \gg \kappa_a$. With a sufficiently high pump rate we obtain the spectra shown in Fig. 5. For both the fundamental and the second-harmonic modes the squeezing is maximum at zero frequency and then degrades with increasing detection frequency in a Lorentzian-like manner excepting the region of excess noise that is due to the laser's relaxation oscillation. Noise features present in the fundamental trace, both relaxation oscillation and squeezing, are present on the second-harmonic trace but are amplified away from the quantum limit.

As we are using a laser model that can produce rate-matched squeezing,¹³ it is necessary to confirm SHG process is indeed the source of the noise suppression. We checked this by turning off the doubling process, by setting χ to zero, and by adjusting the pump rate such that the output power stays the same. We saw a larger relaxation oscillation and no squeezing. The doubling process can significantly damp the relaxation oscillation; a thousandfold reduction is not unusual. By an increase in the pump rate, a small amount of squeezing at low detection frequencies can be created, which is caused by rate matching. In conclusion, the preeminent cause of the squeezing shown in Fig. 5 is the second-harmonic generation.

Figure 6 considers the doubly resonant case in the limit of high pump rate. As was discussed in Subsection 4.A, improved squeezing is expected owing to the oscillation between the fundamental and the second-harmonic modes. However, the changes to the noise spectra are dramatic compared with the passive case. The relaxation oscillation noise of both modes is suppressed, particularly that of the fundamental, and downshifted in frequency. Two regimes of squeezing become evident, that before and that after the relaxation oscillation; hence they are called low and high frequency, respectively. The second-harmonic low-frequency squeezing increases significantly and attains the maximum possible value of 1/2 at zero frequency. Likewise, the high-frequency squeezing is pushed very close to zero in a broad region that is much larger than even the bandwidth of the second-harmonic cavity. Both the high- and the low-frequency squeezing regimes have been described separately in previous works. The value of Fig. 6 is twofold: It demonstrates both regimes can coexist for the one parameter set, and it highlights the relationship between them.

2. Squeezing of the Fundamental Light

Consider, as in Fig. 7, an active doubler resonant at the second harmonic (the bad-cavity limit for ω), $\kappa_a \gg \kappa_c$. A high pump is necessary simply to allow lasing. As the interaction is strong, both the low- and the high-squeezing regimes are evident (c.f. Fig. 5); however, unlike the second-harmonic case, the noise features of the

second harmonic are no longer amplified versions of those of the fundamental. The low-frequency squeezing of the fundamental is less than that of the second harmonic; the high-frequency squeezing is greater.

In the doubly resonant case, $\kappa_a > \kappa_c$, the low-frequency squeezing tends to be buried under the relaxation oscillation, and it is not robust compared with the second-harmonic case. Although the high-frequency squeezing survives, further consideration of this case is omitted for reasons explained in Subsection 4.C.

C. Effect of Nonzero γ_p

In the previous subsections the atomic dephasing (the decay rate of the lasing coherence), γ_p , was considered to be zero. In solid-state systems, such as Nd:YAG, this is not even approximately true, as there is a large dephasing

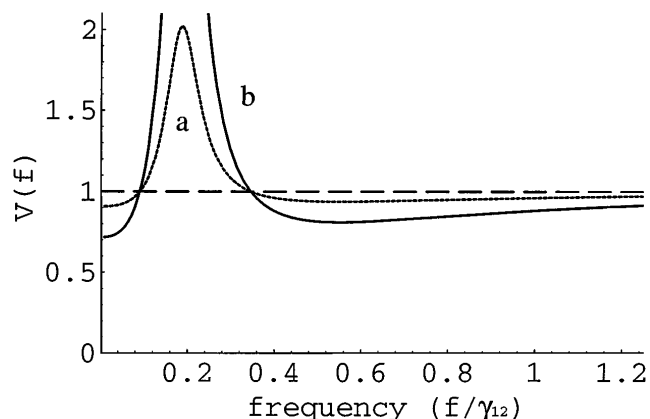


Fig. 5. Spectra for active SHG in the singly resonant case. The parameters are optimized to squeeze the second harmonic, i.e., $\kappa_c \gg \kappa_a$, where $\kappa_a = 0.6\gamma_{12}$ and $\kappa_c = 36000\gamma_{12}$, scaled nonlinearity $\chi = 50000$ (approximately 5220 s^{-1} unscaled), pump rate $\Gamma = 8 \times 10^{-5}\gamma_{12}$ ($\Gamma_{\text{thresh}} = 4.08 \times 10^{-9}\gamma_{12}$), and dephasing rate $\gamma_p = 0$. a, Dashed curve, fundamental spectrum. b, Solid curve, second-harmonic spectrum. Noise features that are present on the fundamental, both relaxation oscillation and squeezing, are amplified away from the quantum limit.

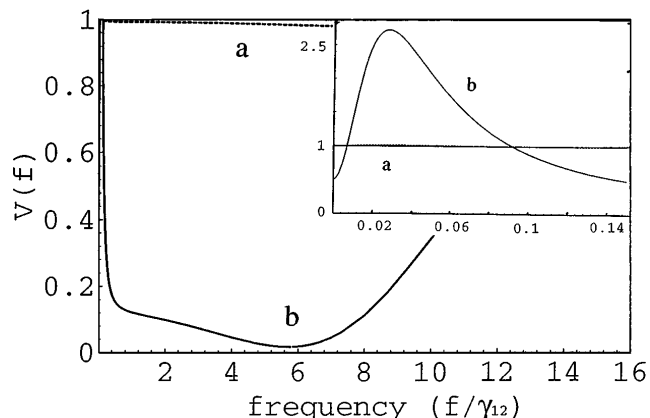


Fig. 6. Spectra for active SHG in the doubly resonant case. There are two plots, covering different frequency ranges. The parameters are optimized to squeeze the second harmonic and are as for Fig. 5 except here $\kappa_c = 36\gamma_{12}$. a, Dashed curve, fundamental spectrum; b, Solid curve, second-harmonic spectrum. Note the two regions of squeezing: low frequency, before the relaxation oscillation, with maximum squeezing of 0.5; and high frequency, above the relaxation oscillation frequency, with maximum squeezing of almost zero.

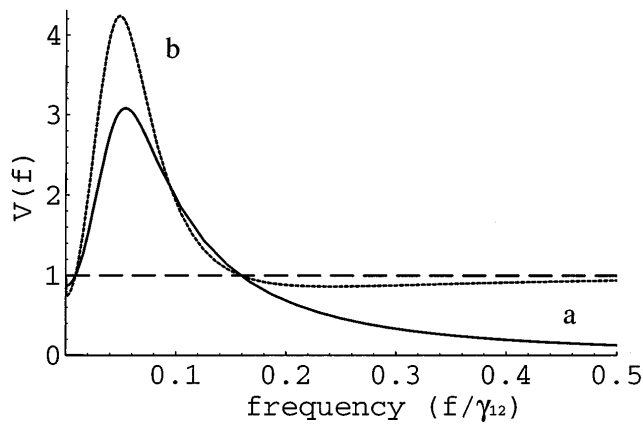


Fig. 7. Spectra for active SHG in the doubly resonant case. The parameters are optimized to squeeze the fundamental, i.e., $\kappa_a > \kappa_c$, where $\kappa_a = 3600\gamma_{12}$ and $\kappa_c = 0.6\gamma_{12}$, $\chi = 50000$, pump rate $\Gamma = 3.99 \times 10^{-2}\gamma_{12}$ ($\Gamma_{\text{thresh}} = 2.92 \times 10^{-5}\gamma_{12}$), and dephasing rate $\gamma_p = 0$. a, Solid curve, fundamental spectrum. Both the relaxation oscillation and the squeezing at low frequencies of the fundamental is less than the second harmonic. b, Dashed curve, second-harmonic spectrum.

value because of coupling between phonons of the crystal and the energy levels of the laser. Even in gas lasers, the dephasing rate is high owing to collisional processes. What, then, is the effect of large γ_p ?

In the passive case the output spectrum of the laser becomes noisier: The relaxation oscillation is down shifted in frequency, and it is amplified, even at high frequencies in the very tail of the oscillation. The extra pump noise leads to a further degradation of squeezing, as the minimum point of the spectrum is reduced and moved up in frequency by a small amount. The effect is minimal.

In the active case, increasing γ_p has notable effect. The laser threshold increases; the critical-point threshold decreases, in some parameter regimes it is lower than the laser threshold, and the system is consequently unstable; and considerable noise is introduced at frequencies below the dephasing value. The squeezing on the fundamental is particularly sensitive, with even low dephasing values, such as $\gamma_p = 0.5 \kappa_a$, completely masking the squeezing. The squeezing of the second harmonic survives, albeit in a somewhat unlikely regime. This is illustrated in Fig. 8, in which the singly resonant system of Fig. 6 is evaluated for dephasing values of γ_p equal to 0, $18\gamma_{12}$, and $0.97\gamma_{12}$, which corresponds to γ_p equal to $0.97\kappa_c$. Note that the degradation of the low-frequency squeezing is much less pronounced and that it does not visibly degrade between the latter two values of γ_p .

This behavior is perhaps best considered as follows. Dephasing adds considerable phase noise inside the laser cavity, which is added directly to the fundamental and is consequently transmitted to the second harmonic. The survival of the low-frequency second-harmonic amplitude squeezing reflects the fact that, when using direct detection, one sees only amplitude noise at zero frequency. However, at higher frequencies the cavity mixes in the internal phase noise. Thus the higher the dephasing rate, the narrower the region of squeezing, as the phase noise at a given frequency is stronger. Since the parametric process also takes place in second-harmonic generation,

the phase noise on the second-harmonic generates additional amplitude noise on the fundamental. As a consequence, none of the low-frequency fundamental squeezing survives.

Contrast this with the passive case. Here the internal phase noise of the laser is not directly involved in the doubling process. The narrow output linewidth of the laser filters the phase noise considerably; consequently, only a relatively small amount of excess noise is added to the pump.

It should be noted that the dephasing rate of Nd:YAG at room temperature is much higher than the values considered in Fig. 8: we approximate it in this paper by $\gamma_p = 9000\gamma_{12}$. At this value the high-frequency squeezing for

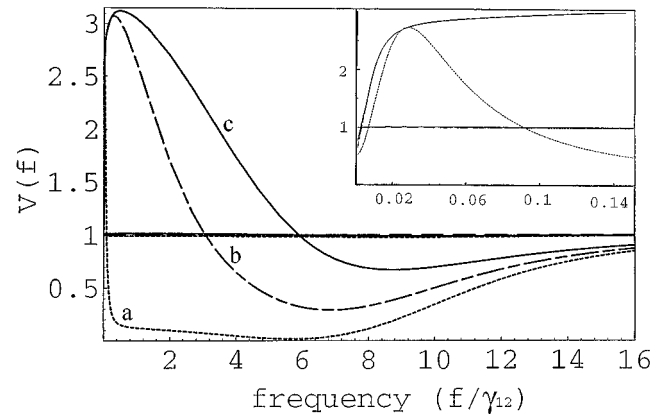


Fig. 8. Spectra showing the effect of nonzero dephasing on active SHG, with squeezing optimized for the second harmonic. Excepting the dephasing rates, other parameters are as for Fig. 6. There are two plots, covering different frequency ranges. For a–c, the significantly squeezed trace is the second harmonic. a, Dotted curves, fundamental and second-harmonic spectra for $\gamma_p = 0$. b, Long-short-dashed curves, fundamental and second-harmonic spectra for $\gamma_p = 18\gamma_{12}$. Both the low- and the high-frequency squeezing is degraded. c, Solid curves, fundamental and second-harmonic spectra for $\gamma_p = 35\gamma_{12}$. Compared with b, the high-frequency squeezing is further degraded, whereas the low-frequency squeezing is much less affected.

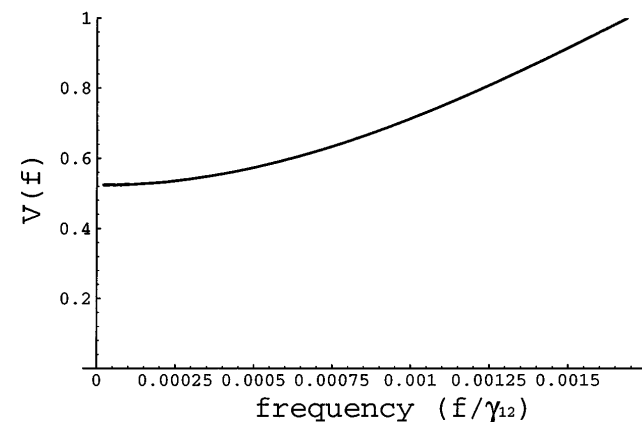


Fig. 9. Demonstration that, in the active case, low-frequency squeezing of the second harmonic is possible even with very high dephasing. The parameters are as for Fig. 6, except here $\gamma_p = 9000\gamma_{12}$ and pump rate $\Gamma = 1.8 \times 10^{-5}\gamma_{12}$. Our model does not include pump noise of the laser, which in real systems will totally mask this effect.

both the active fundamental and the second-harmonic cases is destroyed, as classical noise is introduced at frequencies $< 9000\gamma_{12}$ (300 GHz). To access this squeezing in the laboratory, one must find a way of reducing γ_p , either through judicious choice of the medium or cooling.

Theoretically the low-frequency squeezing of the second harmonic persists even for this value of the dephasing. To understand this, consider the system discussed for Fig. 6 except with dephasing rate $\gamma_p = 9000\gamma_{12}$ and pump rate $\Gamma = 1.8 \times 10^{-5}\gamma_{12}$. This is illustrated in Fig. 9. Squeezing near the 50% limit occurs at zero frequency, but it degrades quickly with increasing detection frequency to the quantum limit (by 56 kHz). It should be stressed that our laser model ignores both pump noise for the laser and thermal noise, which in real lasers raises the noise floor at low frequencies, masking this effect completely. In addition, unrealistically high pump powers are required, or alternatively, a system with an extremely low threshold.

5. SUMMARY

A. Squeezing with Passive Second-Harmonic Generation

Passive second-harmonic generation is already used as a source of bright squeezed light. As reported elsewhere,⁶ there is excellent quantitative agreement between the passive model presented here and experiments. Thus we confidently predict significant improvement in squeezing in present experiments by reduction of the pump noise. Ideally this is achieved by lasers with a narrower amplitude noise linewidth; because such systems are not readily available, an alternative is to place a narrow-linewidth mode-cleaning between the laser and the SHG system. It is interesting to contemplate whether recent results obtained in the rather different field of passive traveling-

wave SHG need be considered in light of the pump noise coupling.²³

The issue of pump noise aside, there is likely to be further, notable, improvement in passive squeezing owing to technological advances. The effective interaction can be further improved by use of materials with a higher nonlinearity (such as KNbO₃), by use of a lower absorptive loss, which is a significant limit to the circulating intracavity power and thus the interaction, or both. To date, detection efficiencies often have limit measurements, particularly in the visible; however, the recent report²⁴ of very-high quantum-efficiency detectors suggests this restriction may soon be relaxed. In the future, reliable doubly resonant systems, probably based on the hemilithic cavity, should overcome the current locking difficulties and allow tailored squeezing, i.e., large values at nonzero frequencies. The prospects for squeezing with passive SHG are bright.

B. Squeezing with Active Second-Harmonic Generation

Although active SHG is experimentally attractive and other analyses have found the theoretical potential to be high, we find here that active SHG is not a suitable source of squeezed light. This is primarily because of the high dephasing values that are inherent in most layer systems: Only if an active system with small dephasing can be found would active SHG be suitable for squeezing. Even then, the issue of high pump rates would need to be addressed. Unfortunately, any of these options offers experimental complications at least as large as that of doubly resonant passive SHG and with no extra benefit as regards the squeezing.

APPENDIX A

For the passive case the drift, A , and the diffusion, D , matrices are, respectively,

$A[1, 1] = \kappa_a$	$A[2, 2] = \kappa_a$	$A[7, 1] = -g_{23}(J_3 - J_2)$
$A[1, 7] = -g_{23}$	$A[2, 10] = -g_{23}$	$A[7, 7] = (\gamma_{13} + \gamma_{23} + \gamma_{12} + 2\gamma_p)/2$
		$A[7, 9] = g_{23}a$
$A[9, 1] = g_{23}J_{23}$	$A[8, 1] = g_{23}J_{23}$	$A[10, 2] = -g_{23}(J_3 - J_2)$
$A[9, 2] = g_{23}J_{23}$	$A[8, 2] = g_{23}J_{23}$	$A[10, 9] = g_{23}a$
$A[9, 7] = g_{23}a$	$A[8, 7] = g_{23}a$	$A[10, 10] = (\gamma_{13} + \gamma_{23} + \gamma_{12} + 2\gamma_p)/2$
$A[9, 8] = -\gamma_{23} - \gamma_{13}$	$A[8, 8] = \Gamma + \gamma_{23} + \gamma_{13}$	
$A[9, 9] = \gamma_{12}$	$A[8, 9] = \Gamma$	$A[3, 1] = 2(\kappa_a\kappa_b)^{0.5}$
$A[9, 10] = g_{23}a$	$A[8, 10] = g_{23}a$	$A[3, 3] = \kappa_b$
$A[4, 2] = 2(\kappa_a\kappa_b)^{0.5}$	$A[6, 4] = \chi b^*$	$A[3, 4] = -\chi c$
$A[4, 3] = -\chi c^*$	$A[6, 6] = \kappa_c$	$A[3, 5] = -\chi b^*$
$A[4, 4] = \kappa_b$		$A[5, 5] = \kappa_c$
$A[4, 6] = -\chi b$	$A[5, 3] = \chi b$	
$D[3, 3] = \chi c$	$D[7, 7] = g_{23}2J_{23}a$	
$D[4, 4] = \chi c^*$	$D[7, 10] = \Gamma(\sigma_1) + (1 + 2\gamma_p)\sigma_3$	
$D[9, 9] = -g_{23}2J_{23}a + \gamma_{12}J_2 + \gamma_{23}J_3$	$D[8, 8] = -g_{23}2J_{23}a + \gamma_{23}J_3 + \Gamma J_1 + \gamma_{13}J_3$	
$D[10, 9] = -\gamma_{12}J_{23} = D[7, 9]$	$D[8, 9] = -g_{23}2J_{23}a - \gamma_{23}J_3$	
$D[10, 10] = g_{23}2\sigma_{23}a$		

For the active case the drift, A , and the diffusion, D , matrices are, respectively,

$A[1, 1] = \kappa_b$ $A[1, 2] = -\chi c^*$ $A[1, 3] = -\chi a$ $A[1, 5] = -g_{23}$ $A[2, 1] = -\chi c$ $A[2, 2] = \kappa_b$ $A[2, 4] = -\chi a$ $A[2, 8] = -g_{23}$ $A[3, 1] = \chi a$ $A[3, 3] = \kappa_c$ $D[1, 1] = \chi c$ $D[2, 2] = \chi c$ $D[6, 7] = -g_{23}2J_{23}a - \gamma_{23}J_3$	$A[4, 2] = \chi a$ $A[4, 4] = \kappa_c$ $A[5, 1] = -g_{23}(J_3 - J_2)$ $A[5, 5] = (\gamma_{13} + \gamma_{23} + \gamma_{12} + 2\gamma_p)/2$ $A[5, 7] = g_{23}a$ $A[6, 1] = g_{23}J_{23}$ $A[6, 2] = g_{23}J_{23}$ $A[6, 5] = g_{23}a$ $A[6, 6] = \Gamma + \gamma_{12}$ $A[6, 7] = -\Gamma$ $D[5, 5] = g_{23}2J_{23}a$ $D[5, 8] = \Gamma J_1 + \gamma_{12}J_3 + 2\gamma_p J_3$ $D[8, 8] = g_{23}2J_{23}a$	$A[6, 8] = g_{23}a$ $A[7, 1] = g_{23}J_{23}$ $A[7, 2] = g_{23}J_{23}$ $A[7, 5] = g_{23}a$ $A[7, 6] = -\gamma_{23} - \gamma_{13}$ $A[7, 7] = \gamma_{12}$ $A[7, 8] = g_{23}a$ $A[8, 2] = -g_{23}(J_3 - J_2)$ $A[8, 6] = -g_{23}a$ $A[8, 8] = (\gamma_{13} + \gamma_{23} + \gamma_{12} + 2\gamma_p)/2$ $D[7, 5] = -\gamma_{12}J_{23}$ $D[7, 7] = -g_{23}2J_{23}a + \gamma_{12}J_2$ $+ \gamma_{23}J_3$ $D[7, 8] = -\gamma_{12}J_{23}$
--	---	---

ACKNOWLEDGMENTS

The authors are grateful to C. M. Savage, M. S. Taubmann, D. E. McClelland, and M. J. Collett for stimulating conversation regarding this and related work. This research was supported by the Australian Research Council.

REFERENCES

1. P. D. Drummond, K. J. McNeil, and D. F. Walls, *Opt. Acta* **27**, 321 (1980); **28**, 211 (1981).
2. L. A. Lugiato, G. Strini, and F. de Martini, *Opt. Lett.* **8**, 256 (1983).
3. R. Paschotta, M. Collett, P. Kürz, K. Fiedler, H.-A. Bachor, and J. Mlynek, *Phys. Rev. Lett.* **72**, 3807 (1994).
4. P. Kürz, R. Paschotta, K. Fiedler, and J. Mlynek, *Europhys. Lett.* **24**, 449 (1993).
5. A. Sizmann, R. J. Horowicz, G. Wagner, and G. Leuchs, *Opt. Commun.* **80**, 138 (1990).
6. T. C. Ralph, M. S. Taubman, A. G. White, D. E. McClelland, and H.-A. Bachor, *Opt. Lett.* **20**, 1316 (1995).
7. M. Dance, M. J. Collett, and D. F. Walls, *Phys. Rev. A* **48**, 1532 (1993).
8. T. A. B. Kennedy, T. B. Anderson, and D. F. Walls, *Phys. Rev. A* **40**, 1385 (1989).
9. R. Schack, A. Sizmann, and A. Schenzle, *Phys. Rev. A* **43**, 6303 (1991).
10. D. F. Walls, M. J. Collett, and A. S. Lane, *Phys. Rev. A* **42**, 4366 (1990).
11. P. García-Fernández, L. A. Lugiato, F. J. Bermejo, and P. Galatola, *Quantum Opt.* **2**, 49 (1990).
12. R. B. Levien, M. J. Collett, and D. F. Walls, *Phys. Rev. A* **47**, 2324 (1993).
13. T. C. Ralph and C. M. Savage, *Phys. Rev. A* **44**, 7809 (1991).
14. W. H. Louisell, *Quantum Statistical Properties of Radiation* (Wiley, New York, 1973); H. Haken, in *Laser Theory*, Vol. 30/2c of *Encyclopedia of Physics*, S. Flügge, ed., (Springer-Verlag, Heidelberg, 1970).
15. G. J. Milburn, M. D. Levenson, R. M. Shelby, S. H. Perlmuter, R. G. DeVoe, and D. F. Walls, *J. Opt. Soc. Am. B* **4**, 1476 (1987).
16. S. F. Pereira, M. Xiao, H. J. Kimble, and J. L. Hall, *Phys. Rev. A* **38**, 4931 (1988).
17. P. Galatola, L. A. Lugiato, M. G. Porecca, P. Tombesi, and G. Leuchs, *Opt. Commun.* **85**, 95 (1991).
18. H. J. Carmichael, *Phys. Rev. Lett.* **70**, 2273 (1990).
19. C. W. Gardiner, *Phys. Rev. Lett.* **70**, 2269 (1993).
20. P. D. Drummond and D. F. Walls, *Phys. Rev. A* **23**, 2563 (1981).
21. C. W. Gardiner and M. J. Collett, *Phys. Rev. A* **31**, 3761 (1985).
22. A. G. White, M. S. Taubman, T. C. Ralph, P. K. Lam, D. E. McClelland, and H.-A. Bachor, submitted to *Physical Review A*.
23. R. D. Li and P. Kumar, *Opt. Lett.* **18**, 1961 (1993); Z. Y. Ou, *Phys. Rev. A* **49**, 2106 (1994); R. D. Li and P. Kumar, *Phys. Rev. A* **49**, 2157 (1994).
24. P. R. Tapster, J. G. Rarity, and P. C. M. Owens, in *1994 Fifth European Quantum Electronics Conference* (Institute of Electrical and Electronics Engineers, New York, 1994), p. 44.